

Passive seismic data primary estimation and noise removal via focal-denoising closed-loop surface-related multiple elimination based on 3D L1-norm sparse inversion

Wang, Tiexing; Wang, Deli; Sun, Jing; Hu, Bin

DOI

[10.1111/1365-2478.13034](https://doi.org/10.1111/1365-2478.13034)

Publication date

2020

Document Version

Final published version

Published in

Geophysical Prospecting

Citation (APA)

Wang, T., Wang, D., Sun, J., & Hu, B. (2020). Passive seismic data primary estimation and noise removal via focal-denoising closed-loop surface-related multiple elimination based on 3D L1-norm sparse inversion. *Geophysical Prospecting*, 69(1), 122-138. <https://doi.org/10.1111/1365-2478.13034>

Important note

To cite this publication, please use the final published version (if applicable). Please check the document version above.

Copyright

Other than for strictly personal use, it is not permitted to download, forward or distribute the text or part of it, without the consent of the author(s) and/or copyright holder(s), unless the work is under an open content license such as Creative Commons.

Takedown policy

Please contact us and provide details if you believe this document breaches copyrights. We will remove access to the work immediately and investigate your claim.

Passive seismic data primary estimation and noise removal via focal-denoising closed-loop surface-related multiple elimination based on 3D L1-norm sparse inversion

Tiexing Wang^{1,2*}, Deli Wang², Jing Sun^{2,3} and Bin Hu²

¹Acoustical Wavefield of Imaging, Faculty of Applied Science, Delft University of Technology, Delft, 2628 CJ, The Netherlands, ²College of Geo-exploration Science and Technology, Jilin University, Changchun, 130061, China, and ³Department of Geosciences, University of Oslo, Sem Sælands vei 1, Oslo, 0371, Norway

Received November 2019, revision accepted September 2020

ABSTRACT

Passive seismic has recently attracted a great deal of attention because non-artificial source is used in subsurface imaging. The utilization of passive source is low cost compared with artificial-source exploration. In general, constructing virtual shot gathers by using cross-correlation is a preliminary step in passive seismic data processing, which provides the basis for applying conventional seismic processing methods. However, the subsurface structure is not uniformly illuminated by passive sources, which leads to that the ray path of passive seismic does not fit the hyperbolic hypothesis. Thereby, travel time is incorrect in the virtual shot gathers. Besides, the cross-correlation results are contaminated by incoherent noise since the passive sources are always natural. Such noise is kinematically similar to seismic events and challenging to be attenuated, which will inevitably reduce the accuracy in the subsequent process. Although primary estimation for transient-source seismic data has already been proposed, it is not feasible to noise-source seismic data due to the incoherent noise. To overcome the above problems, we proposed to combine focal transform and local similarity into a highly integrated operator and then added it into the closed-loop surface-related multiple elimination based on the 3D L1-norm sparse inversion framework. Results proved that the method was capable of reliably estimating noise-free primaries and correcting travel time at far offsets for a foresaid virtual shot gathers in a simultaneous closed-loop inversion manner.

Key words: Passive seismic data, Closed-loop SRME, Primary estimation, Focal-denoising, Noise removal.

INTRODUCTION

Passive-source seismic is a novel seismic technique developed in recent years. It does not rely on artificial sources but records seismic waves generated by background noise, microseism or natural earthquake. Such non-artificial sources can give pas-

sive seismic a substantial economic advantage compared with artificial seismic.

In passive seismic exploration, sources are mainly divided into two categories: transient source and noise source (Wapenaar *et al.*, 2008, 2011). The transient source is a modified version of artificial seismic; that is, transient-source wavelet is similar to artificial-source wavelets. However, the noise source is different since its distributions are always random, and firing time is continuous. The difference between the artificial

*E-mail: wang.tiexing1992@hotmail.com

seismic and passive seismic is the position and properties of the source.

For passive seismic data processing, virtual shot gathers are obtained after the interferometry process, and virtual shot gathers are kinematically similar to artificial seismic data, which both sources and receivers are in the surface. Such similarity provides a theoretical basis for applying traditional seismic methods (e.g. multiple elimination and migration) on virtual shot gathers. This application simplifies the passive data processing and improves the imaging quality.

Seismic interferometry was first introduced by Claerbout (1968), and then further developed by Schuster (2001), Wapenaar (2004) and Vasconcelos and Snieder (2008a, 2008b). Cross-correlation is one of the most commonly used seismic interferometry techniques for passive-source data. The cross-correlation process must fulfil the assumption that subsurface sources have uniformly illuminated the surface in terms of incident angles and strengths (Groenestijn and Verschuur, 2010; Wapenaar *et al.*, 2010a, 2010b). However, this hypothesis is difficult to satisfy in practice.

In the past few years, many effective applications have been made in estimating primaries from transient-source seismic data, and these applications also motivate us to explore more possibilities in the field of noise-source data processing.

Estimation of primaries by sparse inversion (EPSI; Groenestijn and Verschuur, 2009) is a primary estimation technique for artificial-source data. EPSI was first proposed to overcome the limitations of surface-related multiple elimination (SRME; Verschuur *et al.*, 1992; Berkhout and Verschuur, 1997). In EPSI, a large-scale inversion manner is used to estimate the primaries with a careful selection of the initial primary response in advance. Van Groenestijn and Verschuur (2010) developed a modified version and extended EPSI to transient-source data. In modified EPSI, the surface is not necessary to be illuminated by passive sources, but virtual shot gathers must be the input of the whole procedure. Feng *et al.* (2013) added 3D curvelet representation into robust EPSI (Lin and Herrmann, 2010, 2013) and thereby improved the process precision for artificial-source data. Cheng *et al.* (2015) extended robust EPSI to transient-source data and stabilized the inversion process. After some modifications, EPSI and robust EPSI can handle primary estimation for transient-source data. However, note that both methods cannot reconstruct the correct travel time at far offsets of the transient-source seismic data (Van Groenestijn and Verschuur, 2010).

Moreover, EPSI or robust EPSI for transient-source seismic data are not feasible to primary estimation from the noise-source seismic data. In noise-source seismic data, due to the

incoherent noise, it is almost impossible to choose a proper time window with accurate primary arrival time and appropriate inversion parameters. Besides, incoherent noise damages the primary–multiple model because most of the seismic events are overlapped by the incoherent noise (Berkhout, 1982). These problems will lead to ineffective primary estimation. Hence, we intend to choose a more advanced method: closed-loop SRME based on the 3D L1-norm sparse inversion (sparse closed-loop SRME; Wang *et al.*, 2017), being the basis of the proposed method in this paper.

In 2015, Lopez and Verschuur developed a further advanced primary estimation method called closed-loop SRME. It combines the robustness of SRME and a large-scale parameterization inversion manner of EPSI. This new approach overcomes the limitations of SRME and EPSI, estimating primaries with a powerful constraint in a more reliable and stable way. In another parameterized way, Wang *et al.* (2017) developed closed-loop SRME based on the 3D L1-norm sparse inversion (sparse closed-loop SRME). The conventional closed-loop SRME (Lopez and Verschuur, 2014, 2015) is modified by using a bi-convex optimization to solve the primary–multiple objective function and introducing 3D sparse transform to the constraint condition. Thus, primaries are estimated more accurately, especially in deep data. However, the above-mentioned closed-loop SRME methods can only be applied to the artificial-source data primary estimation. Considering the characteristics of noise-source seismic data, we need to add some modifications to sparse closed-loop SRME, to remove the incoherent noise and reconstruct travel time at far offsets from noise-source data.

To remove noise and reconstruct data, Berkhout and Verschuur (2006) proposed to use focal transform to process artificial-source data. Due to the amplitudes and phases irrelevance of signals and noise, seismic signal and noise are readily separated in the focal domain. In 2007, Fomel proposed to use a concept of local attributes to measure the signal characteristics in a local neighbourhood around each grid point. Additionally, Fomel (2007) modified the definition of instantaneous frequency to local frequency, recognizing it as a form of regularized inversion and then changing regularization to constrain the continuity and smoothness of the output. The same idea is extended to define the local correlation. Then, a noise attenuation framework including local similarity and weighting operator was proposed and has been applied in many fields (Chen and Fomel, 2014; Hu *et al.*, 2019)

In this paper, we use focal transform and local similarity to build to a focal-denoising operator and then add it into the sparse closed-loop SRME framework. After the above

modifications, new sparse closed-loop SRME for passive seismic data is proposed, and clean primaries are estimated directly with correct time from noise-source seismic data.

This paper is organized as follows. In the first section, a brief description of the closed-loop SRME on 3D L1-norm sparse inversion will be given, followed by a definition of the new 3D constraint operator—a combination of 2D curvelet and 1D wavelet. In the second section, we will introduce the theory of seismic denoising by focal transform and local similarity. then, we will describe how we modify sparse closed-loop SRME into a useful tool for noise-source data primary estimation. Finally, to demonstrate the algorithm, we will first show how focal transform and local similarity integrally work by a data test, and then apply the proposed method and sparse closed-loop SRME on passive-source data and artificial-source data, respectively.

THEORIES AND METHODS

Closed-loop surface-related multiple elimination based on 3D L1-norm sparse inversion

Following Lopez and Verschuur (2015), let \mathbf{P} describe the upgoing wavefield at the surface

$$\mathbf{P} = \mathbf{P}_0(\mathbf{I} + \mathbf{A}\mathbf{P}), \quad (1)$$

where \mathbf{P}_0 represents the primary wavefield. Strictly speaking, \mathbf{P}_0 denotes all wavefields that are not related to a reflection at the surface. Thus, primary wavefield here refers to the real primaries, internal multiples, and other wavefields for which all reflection points are not at the surface; \mathbf{I} represents an identity operator whose dimensions are the same as \mathbf{P} ; $\mathbf{A} = \mathbf{S}^{-1} \mathbf{R}$ represents the surface operator, in which \mathbf{S} represents the source matrix from all shots and \mathbf{R} represents the reflection operator of the free surface. We assume that all shots have the same constant source wavelets, denoted by $\mathbf{S} = S(\omega)\mathbf{I}$. The reflection coefficient of the free surface \mathbf{R} is considered as -1 . Therefore, the reflectivity matrix becomes $\mathbf{R} = -\mathbf{I}$. Then, surface operator \mathbf{A} is rewritten as $\mathbf{A} = -\mathbf{S}^{-1}$. In this way, the total upgoing wavefield \mathbf{P} is expressed as the product of the primary wavefield \mathbf{P}_0 and the downgoing wavefield $(\mathbf{I} + \mathbf{A}\mathbf{P})$. Note that each bold capital letter in this paper represents a so-called data matrix in the frequency domain. Every row of the matrix represents a common receiver gather, and every column of the matrix represents a common shot gather (Berkhout, 1982).

We now modify the notation of conventional closed-loop surface-related multiple elimination (SRME) into the form of linear inversion optimization, indicated by linear operator

multiplication (Wang *et al.*, 2017). Then the total wavefield \mathbf{P} can be reformulated as

$$\mathbf{p} = \mathbf{L}\mathbf{p}_0 = f_t^* \text{Blockdiag}_\omega [(\mathbf{I} + \mathbf{A}\mathbf{P})^* \otimes \mathbf{I}] f_t \mathbf{p}_0, \quad (2)$$

where \mathbf{p} and \mathbf{p}_0 represent the total wavefield column vector and primary column vector, respectively; \otimes represents the Kronecker multiplication operator between matrix and vector, and it can convert a matrix–matrix operation into a matrix–vector operation; Blockdiag represents creating a block diagonal matrix in the frequency domain; f_t and f_t^* represent forward Fourier transform and inverse Fourier transform along the time axis, respectively. The physical process in equation (1) can thus be achieved via linear operator multiplication process \mathbf{L} .

Primary estimation is constrained by using a bi-convex L1-norm optimization form (Lin and Herrmann, 2010, 2013):

$$\hat{\mathbf{p}}_0 \leftarrow \underset{\mathbf{p}_0}{\text{argmin}} \|\mathbf{p} - \mathbf{L}\mathbf{p}_0\|_2 \quad \text{s.t.} \quad \|\mathbf{p}_0\|_1 \leq \tau, \quad (3)$$

where $\hat{\mathbf{p}}_0$ represents the estimated primaries column vector and scalar τ represents the L1 norm of the primary \mathbf{p}_0 . The setting of τ is critical for obtaining an accurate primary. If τ is too large, the estimated primaries will not exhibit enough sparseness; if τ is too small, artefacts will be leaked into the estimated primaries due to the incomplete representation during the inversion. The bi-convex optimization shows great stability, because the sets of the objective function and the constraint are both convex, and the local minimum is avoided after the modification to equation (1), i.e. equation (3). That is, we can always obtain a globally optimal solution in equation (3).

The optimization problem in equation (3) can be transformed into (Lin and Herrmann, 2010, 2013)

$$\hat{\mathbf{p}}_0 \leftarrow \underset{\mathbf{p}_0}{\text{argmin}} \|\mathbf{p}_0\|_1 \quad \text{s.t.} \quad \|\mathbf{p} - \mathbf{L}\mathbf{p}_0\|_2 \leq \sigma, \quad (4)$$

where σ represents the residual energy (1%–10% L2 norm of the initial data) between the input data and the total wavefield obtained by estimated primaries. To solve equation (4), we will use a rather beneficial algorithm called the L1-norm spectral gradient projection algorithm (SPGL1; Hennenfent *et al.*, 2008; Berg and Friedlander, 2009, 2011).

After obtaining the estimated primaries $\hat{\mathbf{p}}_0$, surface operator $\hat{\mathbf{A}}$ is calculated by using an L2-norm filter constraint in the time domain:

$$\hat{\mathbf{A}} \leftarrow \underset{\mathbf{A}}{\text{argmin}} \left\| \mathbf{P} - \hat{\mathbf{P}}_0 (\mathbf{I} + \mathbf{A}\mathbf{P}) \right\|_2^2. \quad (5)$$

To improve the estimated result further, a 3D sparse constraint $\mathbf{S} = \mathbf{C}_2 \otimes \mathbf{W}$ is added into the solving process (equation 4). \mathbf{S} is a combination of the 2D curvelet transform \mathbf{C}_2 (Candes and Donoho, 2005) and the discrete wavelet transform using a third-order Battle–Lemarié wavelet \mathbf{W} (Daubechies, 1992). Because of the 3D sparse operator, energy in the shot–receiver domain is sparsified by the 2D curvelet transform, and the 1D wavelet transform is applied along the time axis. In the above 3D sparse domain, the sparse solution is searched during the solving process, by keeping the large sparse coefficients that correspond to primaries and removing the small sparse coefficients that represent to the multiples (Wang *et al.*, 2017)

$$\begin{cases} \hat{\mathbf{s}}_0 \leftarrow \operatorname{argmin}_{\mathbf{s}_0} \|\mathbf{s}_0\|_1 & \text{s.t. } \|\mathbf{p} - \mathbf{L}\mathbf{S}^*\mathbf{s}_0\|_2 \leq \sigma, \\ \hat{\mathbf{p}}_0 \leftarrow \mathbf{S}^*\hat{\mathbf{s}}_0 \end{cases}, \quad (6)$$

where \mathbf{s}_0 represents the sparse coefficients in the 3D sparse domain and \mathbf{S}^* denotes the 3D conjugate operator of \mathbf{S} that can transform the data back to the space-time domain. After alternative inversion, primaries can be estimated by the SPGL1 algorithm mentioned above.

Seismic denoising via focal transform and local similarity

The virtual shot gathers (i.e. cross-correlation result) is the input of our proposed method.

However, there are travel-time errors at far offsets in the virtual shot gathers since the surface is not illuminated from all angles (Groenestijn and Verschuur, 2010; Wapenaar *et al.*, 2010a, 2010b). These errors will decrease the accuracy of subsequent passive seismic data processing if we directly apply the conventional seismic method to passive seismic data (e.g. multiple elimination and velocity analysis). Besides, inheriting from noise-source data, incoherent noise always appears in the virtual shot gathers. Compared with random noise, the morphological characteristics of the incoherent noise is similar to seismic events, resulting in poor performance of conventional seismic denoising methods, additionally making the primary estimation process unstable. Inspired by the successful applications of focal transform (Berkhout and Verschuur, 2006; Lopez and Verschuur, 2015; Ma *et al.*, 2009) and local similarity (Fomel, 2007) in signal restoration and noise removal, we propose an integrated primary estimation process for passive seismic data, together with correcting the travel-time errors at far offsets and thereby compensate the corrected time to the primary estimation results in a closed-loop manner.

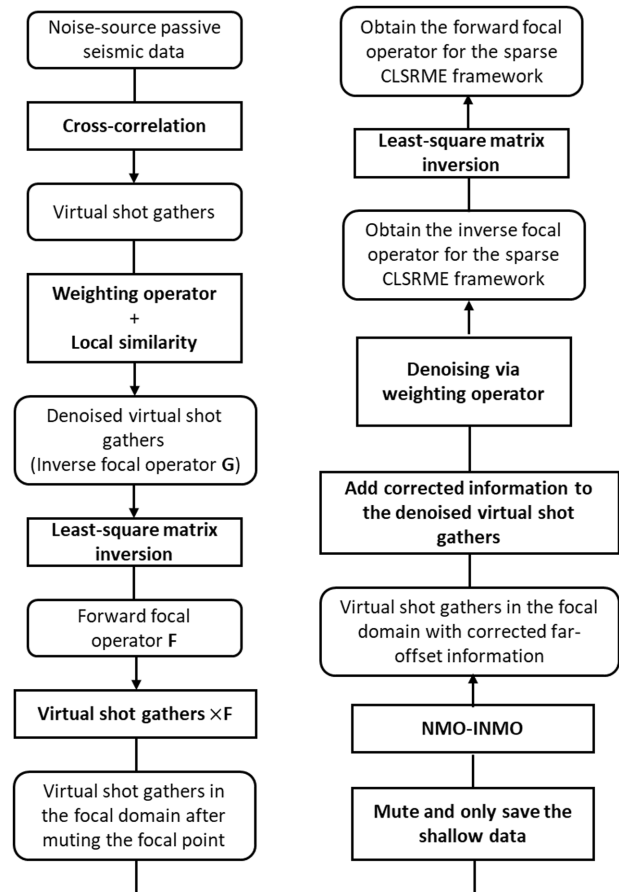


Figure 1 Workflow for obtaining the focal-denoising operator from noise-source passive seismic data.

Review of the focal transform

For denoising, it is common to separate signal and noise in a new data domain by using a suitable mathematical transform. Focal transform is a multishift correlation process, based on a multidimensional operator that contains an estimate of the propagation properties in the subsurface (Berkhout and Verschuur, 2006). By using focal transform, the target signal can be mapped into and around one focal point. In this way, the inverse focal transform is well defined by a multishift convolution process (defocusing). In multiple removal cases, primaries are focused around the zero time, and multiples can be de-ordered into the lower order multiple if we use primaries as the inverse focal operator (Berkhout, 1982; Berkhout and Verschuur, 2006). For example, if we use primaries as the inverse focal operator, first-order multiple and second-order multiple can be de-ordered into primary and first-order multiple, respectively.

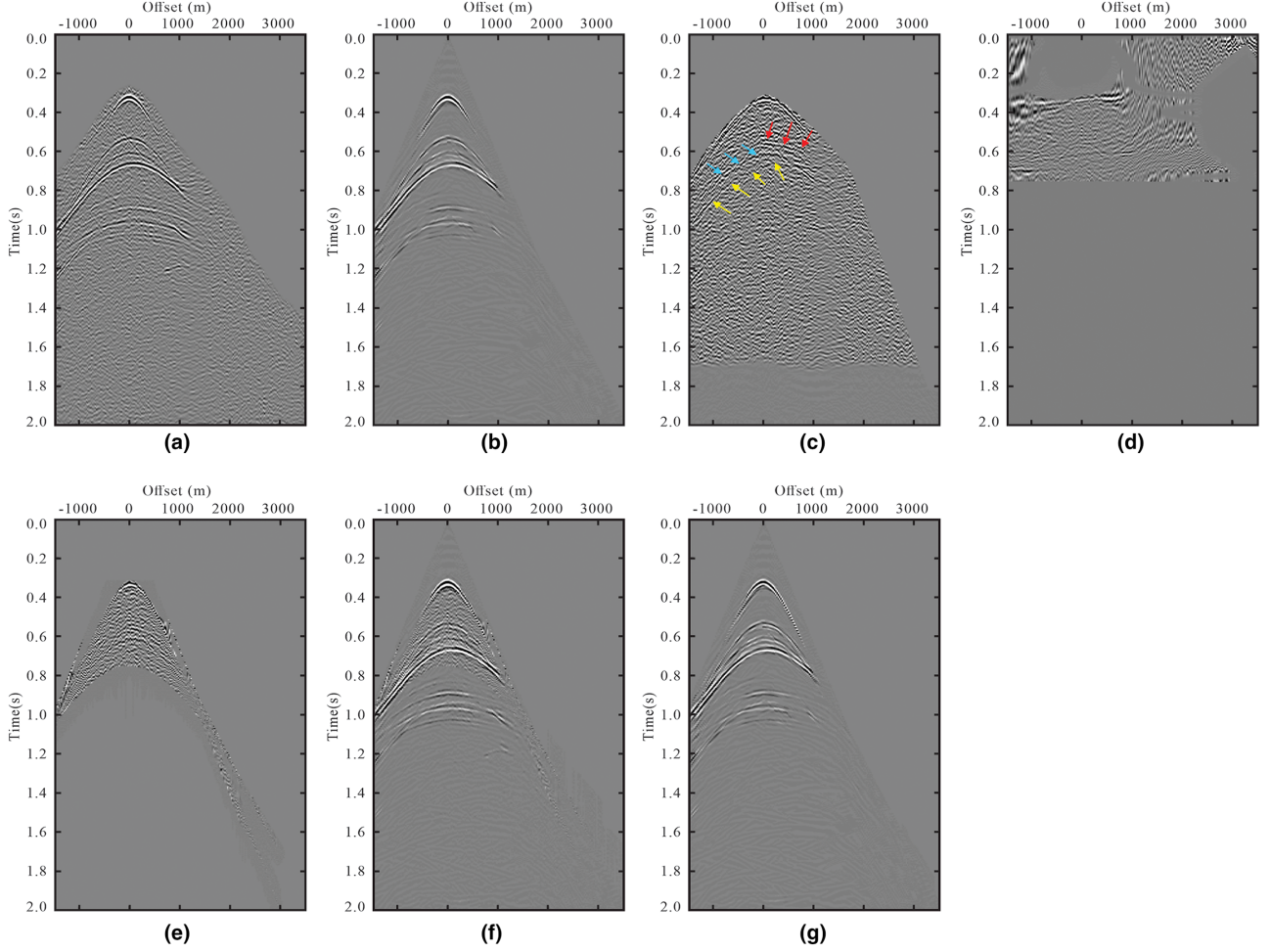


Figure 2 (a) Virtual shot gather obtained from noise-source passive seismic data by cross-correlation, (b) denoised virtual shot gather based on local similarity weighting operator (inverse focal operator), (c) virtual shot gather in the focal domain after muting the focal area, (d) shallow part of Figure 1(a) in the NMO domain, (e) virtual shot gather in the focal domain after correcting the curvatures of events, (f) focal operator with compensated far-offset information and (g) focal operator denoised by the weighting operator.

Following the primary–multiple model proposed by Berkhout and Verschuur (2006), the forward and inverse focal transformation is formulated as a matrix multiplication in each frequency component

$$\mathbf{Q} = \mathbf{F}\mathbf{P} \text{ (forward)} \quad (7)$$

and

$$\mathbf{P} = \mathbf{G}\mathbf{Q} \text{ (inverse)}, \quad (8)$$

where \mathbf{F} and \mathbf{G} are the forward focal operator and the inverse focal operator. With the application of the forward focal transform, the measured data \mathbf{P} can be transferred to \mathbf{Q} in the focal domain (equation (7)). Similarly, inverse focal operator \mathbf{G} can bring \mathbf{Q} back to the original data domain (equation (8)).

The forward focal operator \mathbf{F} can be obtained by an inversion process. One way is to use the least-squares inversion approach (Berkhout and Verschuur, 2006):

$$\mathbf{F} \approx \mathbf{G}^H [\mathbf{G}\mathbf{G}^H + \varepsilon^2 \mathbf{I}]^{-1}, \quad (9)$$

where ε is a stabilization factor. \mathbf{G}^H is a conjugate of the inverse focal operator \mathbf{G} and can remove spatial spectrum from the original seismic records.

Equation (1) describes the physical relationship between primaries and multiples in the frequency domain, which can be further reformulated as

$$\mathbf{P} = \mathbf{P}_0 (\mathbf{I} - \mathbf{A}\mathbf{P}_0)^{-1}, \quad (10)$$

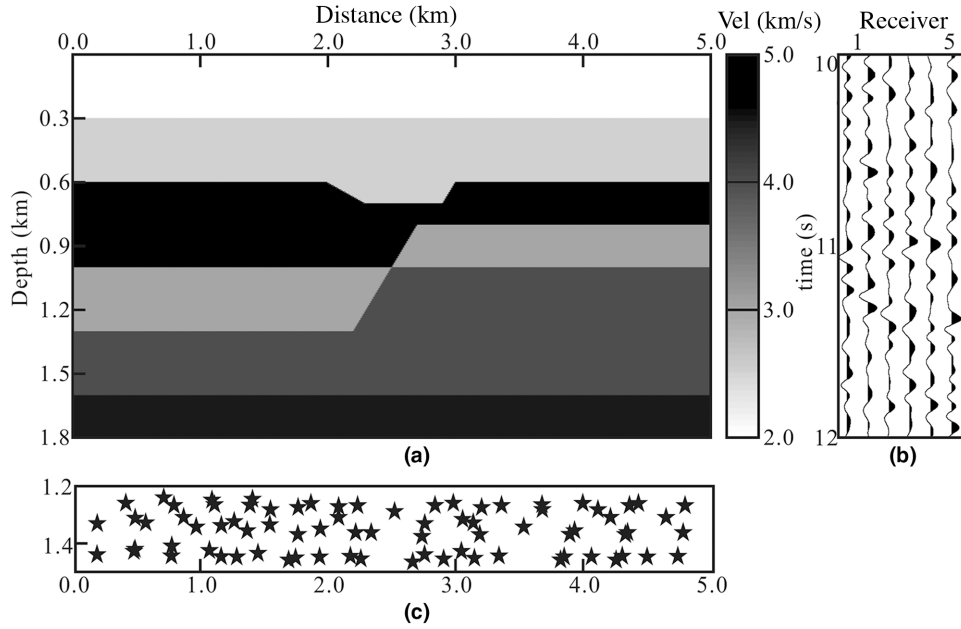


Figure 3 (a) Model for simulating noise-source data and (b) wavelets of the random sources.

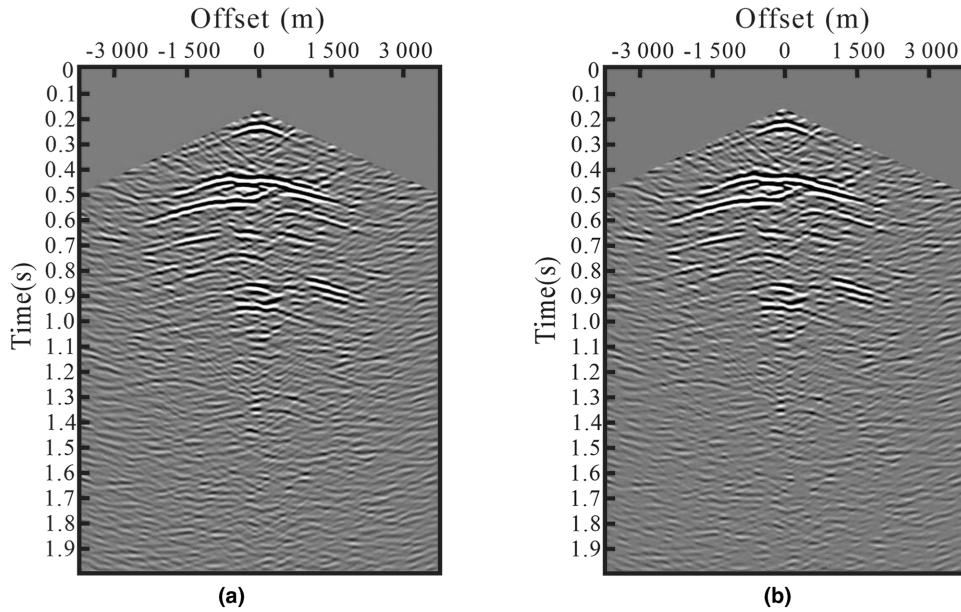


Figure 4 (a) Virtual shot gathers from noise-source seismic data and (b) primary estimation from virtual shot gathers via sparse closed-loop SRME.

Besides, we apply a polynomial expansion on equation (1) (Berkhout, 1982):

$$P = P_0 (I - AP_0 + (AP_0)^2 - (AP_0)^3 + (AP_0)^4 + \dots), \quad (11)$$

$$P = P_0 - P_0AP_0 + P_0(AP_0)^2 - P_0(AP_0)^3 + P_0(AP_0)^4 + \dots, \quad (12)$$

where the acquired seismic wavefield P is the summation of the primary P_0 , the first-order multiple $-P_0AP_0$, the second-order multiple $P_0(AP_0)^2$ and so on.

If we transform the seismic wavefield P to the focal domain and use the primary P_0 as the inverse focal operator G , the forward focal operator F can be calculated as

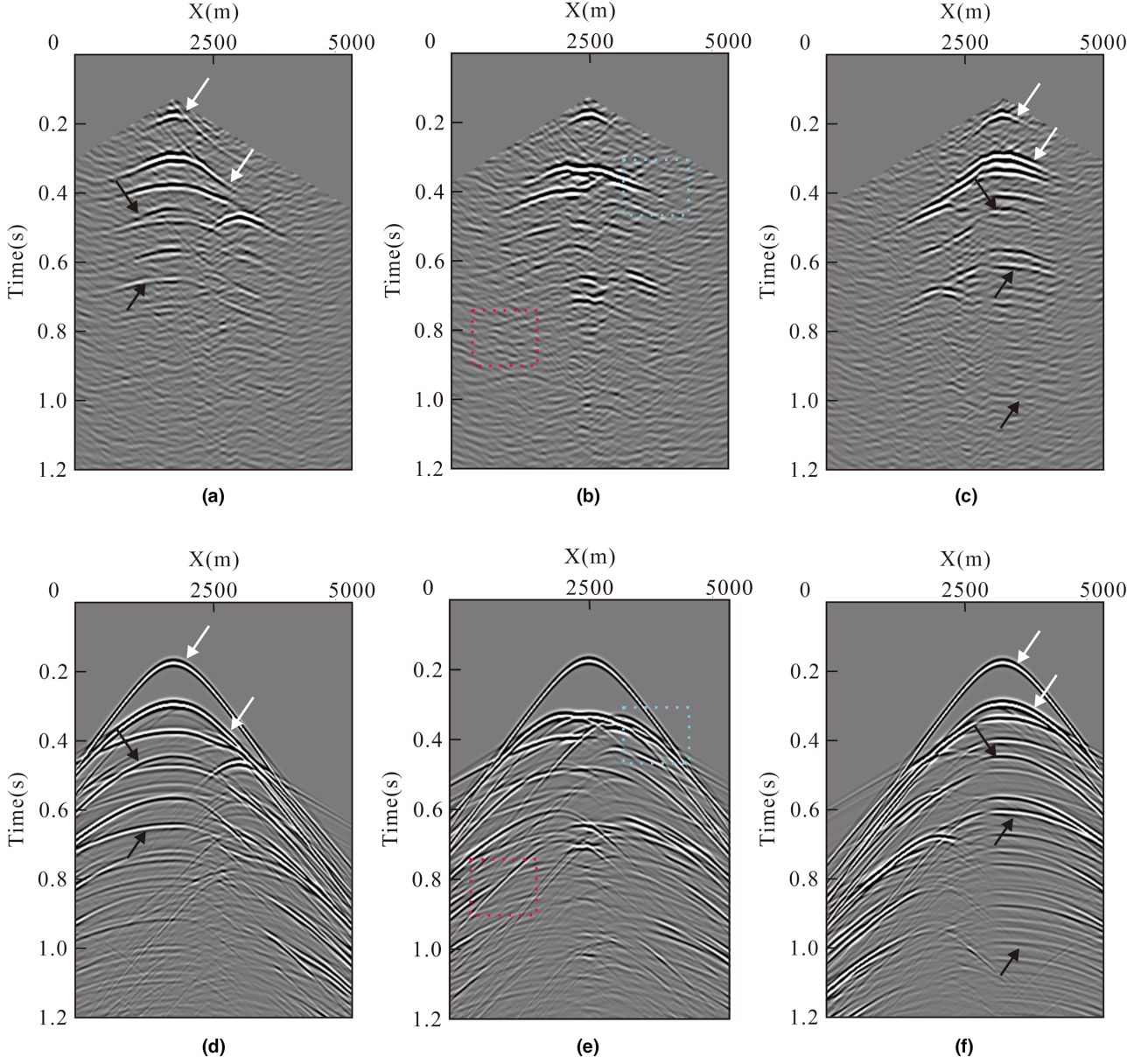


Figure 5 (a–c) Virtual shot gathers from the noise-source data by cross-correlation; (d–f) active-source shot gathers simulated by the same model.

$$\mathbf{F} = \mathbf{P}_0^{-1} \approx \mathbf{P}_0^H [\mathbf{P}_0 \mathbf{P}_0^H + \varepsilon^2 \mathbf{I}]^{-1}. \quad (13)$$

Equation (7) uses the inverse focal operator (equation (13)) together with equation (12) to estimate the acquired seismic wavefield \mathbf{P} in the focal domain:

$$\mathbf{Q}_P = \mathbf{I} - \mathbf{A}\mathbf{P}_0 + (\mathbf{A}\mathbf{P}_0)^2 - (\mathbf{A}\mathbf{P}_0)^3 + (\mathbf{A}\mathbf{P}_0)^4 + \dots \quad (14)$$

and

$$\mathbf{Q}_P = \mathbf{I} - \mathbf{A}(\mathbf{P}_0 - \mathbf{P}_0\mathbf{A}\mathbf{P}_0 + \mathbf{P}_0(\mathbf{A}\mathbf{P}_0)^2 - \mathbf{P}_0(\mathbf{A}\mathbf{P}_0)^3 + \dots). \quad (15)$$

In equations (14) and (15), the primary is represented by \mathbf{I} and localized in the focal domain; the first-order multiple is transformed into the primary; second-order multiple is transformed into the first-order multiple and so on. Forward focal transform is a de-order process, which can raise the valid

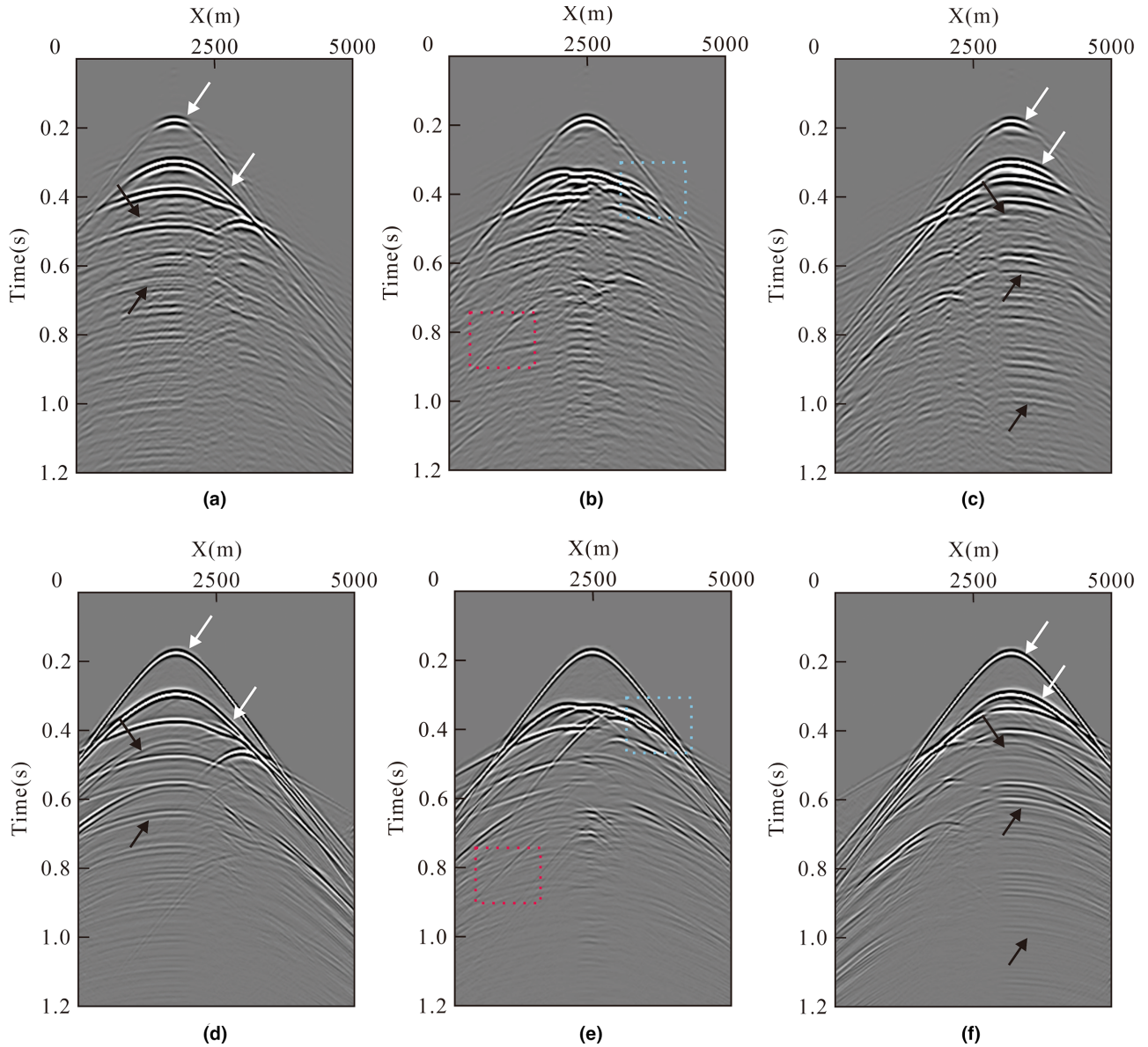


Figure 6 (a–c) Primary estimation results from virtual shot gathers by the proposed method; (d–f) primary estimation results from active-source data by sparse closed-loop SRME.

signal in the deep data to the shallow data in the focal domain. In other words, high-order multiples become low-order multiples or primaries. It provides the basis to extract the correct seismic events at far offsets in the focal domain and compensates the energy into the input data in the normal data domain.

Review of the local similarity

Following Fomel (2007), the local similarity is defined between two vectors \mathbf{a} and \mathbf{b} , vector notations for signal $a(t)$

and $b(t)$:

$$\mathbf{c} = \sqrt{\mathbf{c}_1^T \mathbf{c}_2} \quad (16)$$

where \mathbf{c} is used to describe the degree of local similarity. \mathbf{c}_1 and \mathbf{c}_2 come from the least-squares minimization problem:

$$\mathbf{c}_1 = \operatorname{argmin}_{\mathbf{c}_1} \|\mathbf{A} - \mathbf{C}_1 \mathbf{B}\|_2^2 \quad (17)$$

$$\mathbf{c}_2 = \operatorname{argmin}_{\mathbf{c}_2} \|\mathbf{A} - \mathbf{C}_2 \mathbf{B}\|_2^2, \quad (18)$$

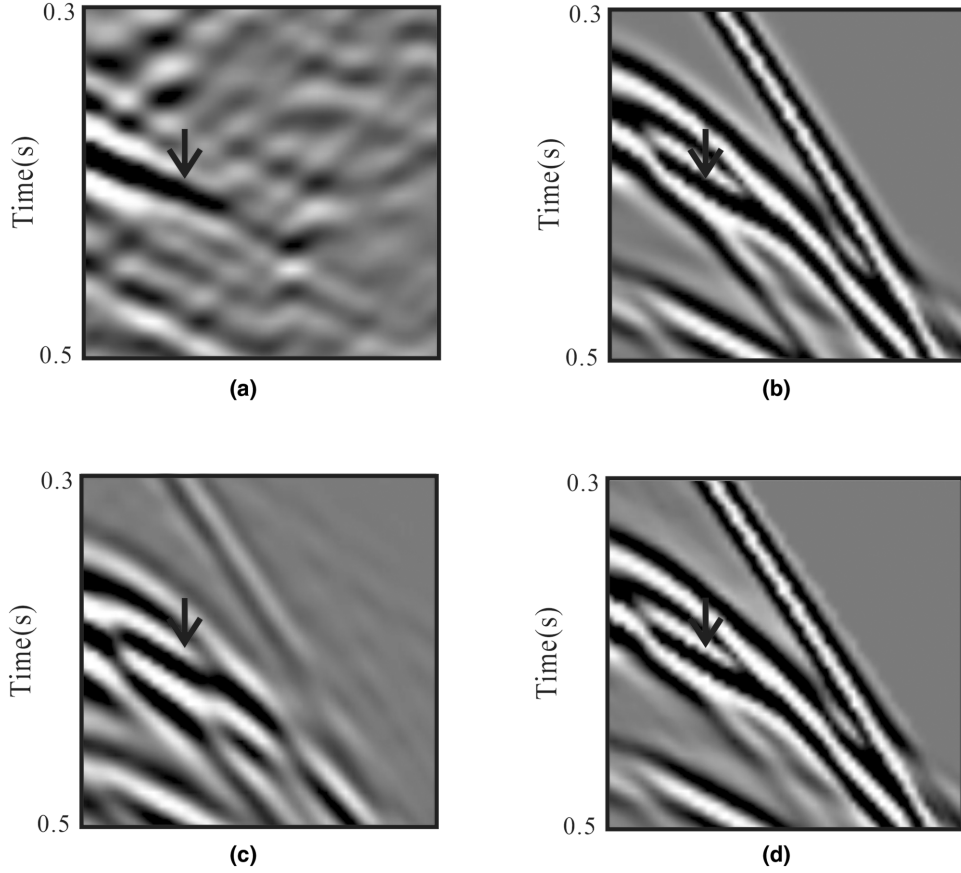


Figure 7 Enlarged portion (red box) of Figures 5(b,e) and 6(b,e).

where \mathbf{A} and \mathbf{B} are diagonal operators composed of the elements of \mathbf{a} and \mathbf{b} , respectively. C_i is a diagonal operator composed from the elements of c_i .

The weighting operator $\mathbf{W}(t, \mathbf{x})$ is defined as

$$\mathbf{W}(t, \mathbf{x}) = \begin{cases} 1 & \text{for } V_{n,s}(t, \mathbf{x}) > v_2 \\ \frac{V_{n,s}(t, \mathbf{x}) - v_1}{v_2 - v_1} & \text{for } v_1 \leq V_{n,s}(t, \mathbf{x}) \leq v_2 \\ 0 & \text{for } V_{n,s}(t, \mathbf{x}) < v_1 \end{cases} \quad (19)$$

to extract reflection information, where $V_{n,s}(t, \mathbf{x})$ represents 2D local similarity coefficients; v_1 and v_2 represent two thresholds and correspond to the fidelity of each noise point as a signal point. s and n represent signal and noise, respectively. The weighting operator $\mathbf{W}(t, \mathbf{x})$ is calculated by detecting a useful component in the noise section with different weighting scales.

FOCAL-DENOISING CLOSED-LOOP SURFACE-RELATED MULTIPLE ELIMINATION BASED ON THE 3D L1-NORM SPARSE INVERSION

To remove noise and reconstruct the correct travel time, we combine the focal transform and local similarity into an integrated process for noise-source data (Fig. 1). We define \mathbf{D} as the focal-denoising operator and then add it into the main loop of the proposed primary estimation method:

$$\begin{cases} \hat{s}_{\text{noise},0} \leftarrow \underset{s_0}{\text{argmin}} \|s_{\text{noise},0}\|_1 & \text{s.t. } \|\mathbf{D}p - \mathbf{DLS}^*s_{\text{noise},0}\|_2 \leq \sigma \\ \hat{p}_{\text{noise},0} \leftarrow \mathbf{S}^*\hat{s}_{\text{noise},0} \end{cases}, \quad (20)$$

where all notations are the same as in equation (6). By using equation (20), we obtain the estimated primaries with less noise and use it as the input for the next loop. After several loops, primaries can be finally estimated without the incoherent noise.

We provide a detailed description of the proposed primary estimation process as follows:

Algorithm: Noise-source data primary estimation and noise removal via focal-denoising closed-loop SRME based on 3D L1-norm sparse inversion

- 1: Input: virtual shot gathers $\mathbf{P}_{\text{noise}}$ from noise-source data obtained by cross-correlation, target residual energy σ (5%-10% of the L2-norm of $\mathbf{P}_{\text{noise}}$);
 - 2: Initialize $\hat{\mathbf{p}}_{\text{noise},0} \leftarrow 0, \hat{A} \leftarrow 0$;
 - 3: Compute $\hat{\mathbf{p}}_{\text{noise},0}$ via $\hat{\mathbf{p}}_0 \leftarrow \operatorname{argmin}_{\mathbf{p}_0} \|\mathbf{p}_0\|_1$
s.t. $\|\mathbf{p} - \mathbf{L}\mathbf{p}_0\|_2 \leq \sigma$,
- Main loop:
- 4: While $i = 1 \rightarrow n_{\text{iter}}$ do
 - 5: if $i < 2$
 - Substitute $\hat{\mathbf{p}}_{\text{noise},0}$ from step 3 into
 - $\hat{A} \leftarrow \operatorname{argmin}_A \|\mathbf{P} - \hat{\mathbf{P}}_0(\mathbf{I} + \mathbf{A}\mathbf{P})\|_2^2$ to calculate \hat{A}_1 ;
 - Reset $\hat{\mathbf{p}}_{\text{noise},0}$ to the zero column vector
 - else
 - Substitute $\hat{\mathbf{p}}_{\text{noise},0}$ into
 - $\hat{A} \leftarrow \operatorname{argmin}_A \|\mathbf{P} - \hat{\mathbf{P}}_0(\mathbf{I} + \mathbf{A}\mathbf{P})\|_2^2$ to calculate \hat{A}_i
 - end
 - 6: Use the estimated primaries to construct the focal-denoising operator;
 - 7: $\begin{cases} \hat{\mathbf{s}}_{\text{noise},0} \leftarrow \operatorname{argmin}_{\mathbf{s}_0} \|\mathbf{s}_{\text{noise},0}\|_1 \text{ s.t. } \|\mathbf{D}\mathbf{p} - \mathbf{D}\mathbf{L}\mathbf{S}^*\mathbf{s}_{\text{noise},0}\|_2 \leq \sigma \\ \hat{\mathbf{p}}_{\text{noise},0} \leftarrow \mathbf{S}^*\hat{\mathbf{s}}_{\text{noise},0} \end{cases}$
 - 8: $i++$
 - 9: until $\|\mathbf{p} - \mathbf{L}\mathbf{S}^*\hat{\mathbf{s}}_{\text{noise},0}\|_2 \leq \sigma$
 - 10: Output: primary estimation results of the original data
 $\mathbf{P}_{\text{noise},0} = \mathbf{S}^*\hat{\mathbf{s}}_{\text{noise},0}$
-

APPLICATION

In this section, we will first give an example to show how the focal transform and local similarity integrally work in the primary estimation process. Then, a simple model data and salt model data are used to demonstrate the proposed method.

Test for focal-denoising operator

To account for the noise removal and travel-time correction capabilities of the focal-denoising operator for passive seismic data, a data test is shown in Figure 2. In Figure 2(a), we can observe that the seismic events and incoherent noise are

mixed with each other, and there are time errors in the virtual shot gathers. To preliminarily attenuate the noise, we use local similarity (Fomel, 2007) combined with the weighting operator (Chen and Fomel, 2014). The denoised result is shown in Figure 2(b). Only seismic events with high amplitudes are preserved after using a large value of the weighting operator. The denoised results (Fig. 2b) are close to the primaries, so we use it as the inverse focal operator \mathbf{G} . In this way, we use inverse focal operator \mathbf{G} and equation (9) to obtain the forward focal operator \mathbf{F} . According to Berkhout and Verschuur (2006), the focal operator can be a single reflector response or multi-reflector responses. In our case, the virtual shot gathers consist of both primaries and multiples. Therefore, primaries in the input data will be mapped in or around the focal point if we only use primaries as the inverse focal operator. Multiples in the focal domain will appear in the positive time axis. We muted the signal around the focal point, and the signal above 0.3 s is muted in our case. The muted area is decided by the first seismic events in Figure 2(a). And the muted result is shown in Figure 2(c). Seismic events indicated by the colourful arrows have similar curvatures with the input data (Fig. 2a). This similarity also demonstrates the kinematical feasibility of the focal transform for passive seismic data.

Although the far offsets (offset: -1200 to -300) have been reconstructed by the focal transform (Fig. 2c), the curvatures of seismic events here are still incorrect. In Figure 2, far offsets are defined by the area, where there are no valid seismic events. For example, in Figure 2(a), we can only observe the first seismic event (0.3 s) from offset -100 to offset 100.

Then, we apply normal move-out and inverse normal move-out (NMO-INMO) on the shallow data (Fig. 2d) to correct the curvatures of the data at far offsets. The definition of the shallow data can be empirical. For example, in Figure 2(c), the shallow part is defined as the area above the 1.0 s events. In terms of NMO speed, we use automatic velocity picking, and the NMO-INMO result is shown in Figure 2(e). Then, we introduce the corrected information (Fig. 2e) into the data (Fig. 2b) and then obtain the focal operator with compensated far offsets (Fig. 2f). By comparing Figure 2(f,g), we can see those seismic events at far offsets have been reconstructed, which means travel-time errors have been corrected. In the actual processing of our proposed method, all the above steps have been integrated into an operator named the focal-denoising operator, which can be added into the sparse closed-loop surface-related multiple elimination (SRME) framework directly. During the inversion process, we use the estimated primaries as the input of the

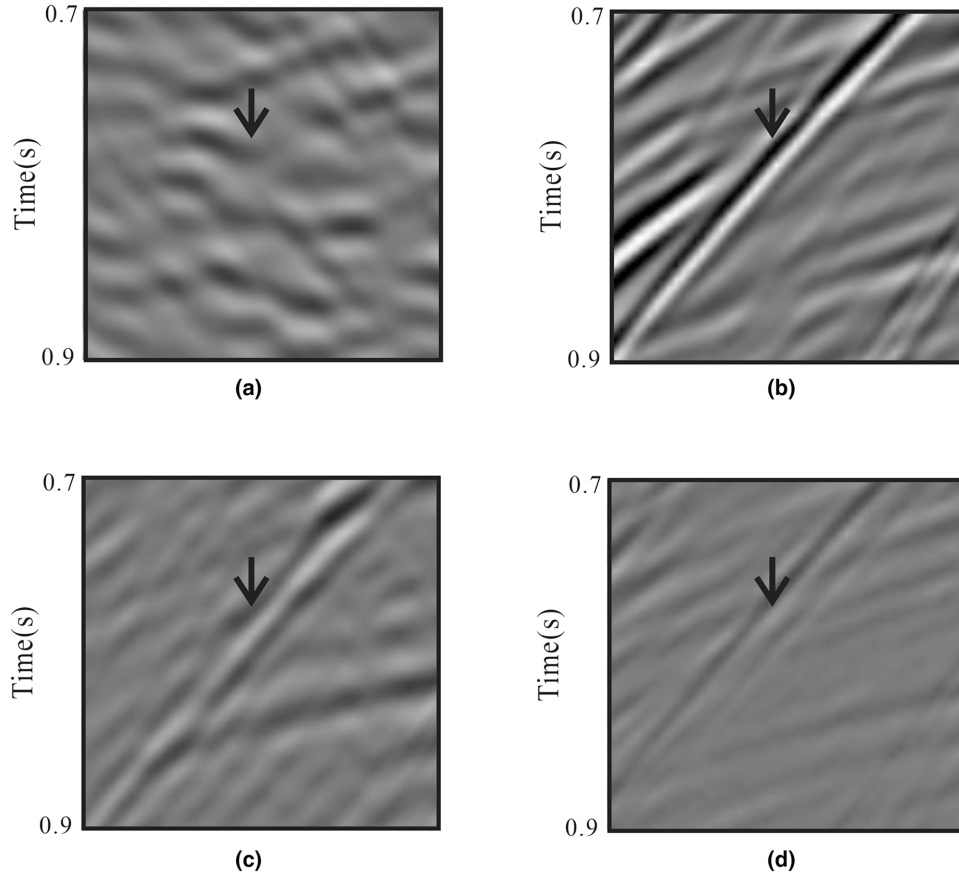


Figure 8 Enlarged portion (blue box) of Figures 5(b,e) and 6(b,e).

focal-denoising operator. Thereby, we can obtain the updated focal operator for the next iteration. In each iteration of closed-loop SRME, the updated focal operator is added into the linear operator inversion process. Consequently, far-offset information is gradually compensated to the final primary estimation result. Noise-free primary estimation and far-offset reconstruction can thus be achieved simultaneously.

Simple model

In this section, we will illustrate the algorithm with a 2D data set obtained from the five-reflector subsurface model with a fault in Figure 3(a). Two hundred and fifty receivers with a 20-m interval are set at the surface, while 299 noise sources emitting random small bursts (Fig. 3b) are randomly buried underground. We obtain 800 seconds passive records for the cross-correlation process and associated virtual shot gathers are shown in Figure 4(a).

To account for the focal-denoising capabilities of the present method, we first estimate primaries (Fig. 4b) from vir-

tual shot gathers (Fig. 4a) via sparse closed-loop SRME. As we can see, multiples have not been eliminated, because incoherent noise is similar to the available seismic events and consequently disturbed the inversion process. Besides, travel-time errors at far offsets and incoherent noise ruin the primary-multiple model (Berkhout, 1982). From Figure 4, we can conclude that it is impossible to apply sparse closed-loop SRME in this circumstance, and the introduction of the focal-denoising operator to the sparse closed-loop SRME framework is necessary.

To test the effectiveness of the present method further, the active-source acquisition is also set for the same model as a reference. Figure 5(d–f) shows the artificial-source shot gathers from the simple model (Fig. 3a). By comparing virtual shot gathers (Fig. 5a–c) and active-source shot gathers (Fig. 5d–f), we can observe that travel times (curvature of the events) are incorrect in the virtual shot gathers (white arrows). This occurs because the subsurface sources cannot illuminate the surface with all angles. Besides, seismic events are overlapped by incoherent noise (black arrows) at 0.8 to 1.2 s in Figure 5(a–c).

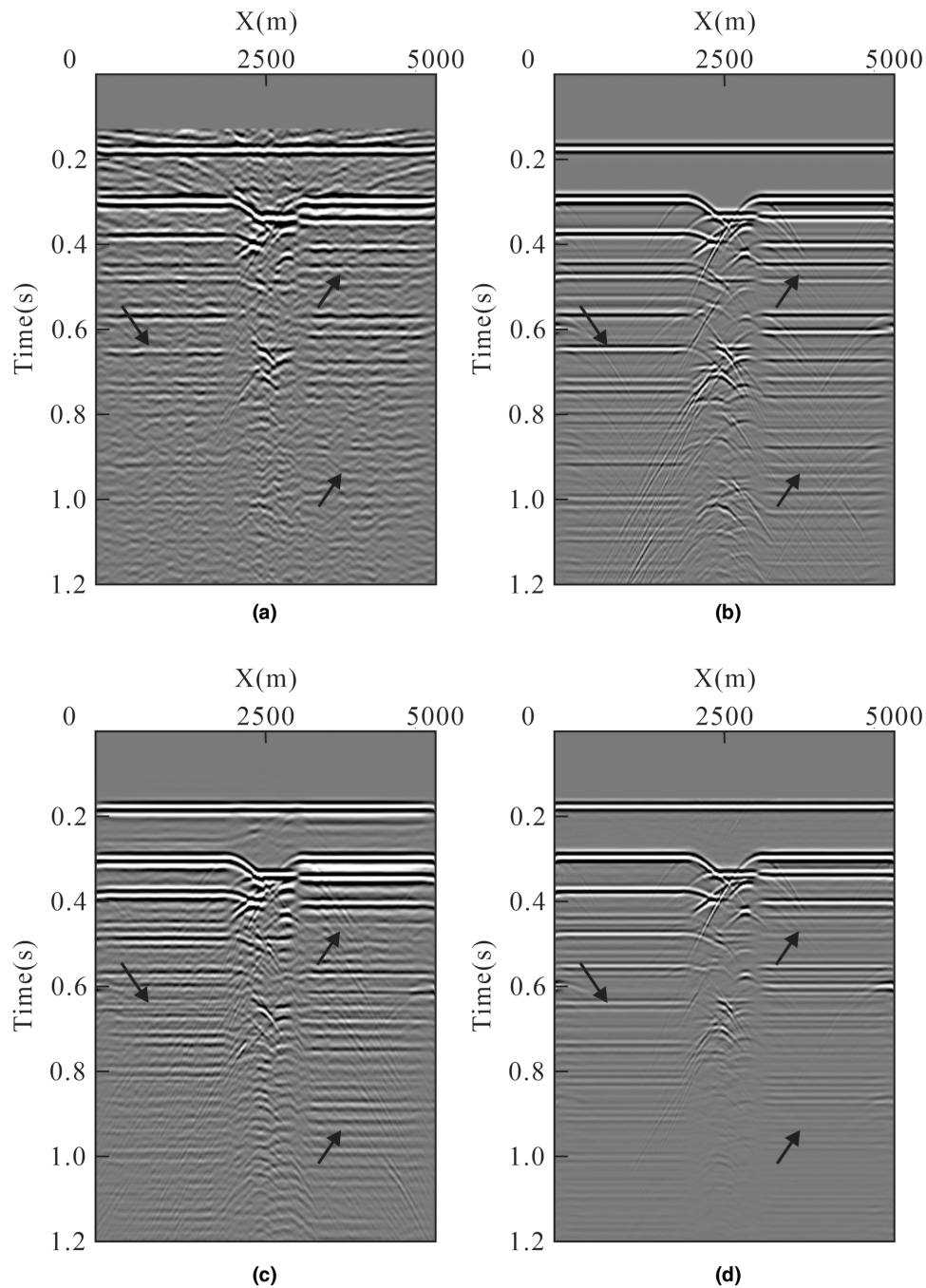


Figure 9 Zero-offset profile of (a) virtual shot gathers obtained from noise-source data by cross-correlation, (b) active-source data, (c) estimated primaries from noise-source data by the proposed method and (d) estimated primaries from active-source data by sparse closed-loop SRME.

Figure 6(a–c) depicts the primary estimation results from noise-source data by using the proposed method. To better account for the capabilities of the algorithm, we use sparse closed-loop SRME to estimate primaries from artificial-source shot gathers (Fig. 6d–f). By comparing the input (Fig. 5a–

c) and the output (Fig. 6a–c) data sets, we can see that incoherent noise has been removed (also shown in Fig. 8). Additionally, travel-time errors correction (white arrows) and multiple elimination (black arrows) have been achieved (Figs 5–7). To further demonstrate the result quantitatively, we

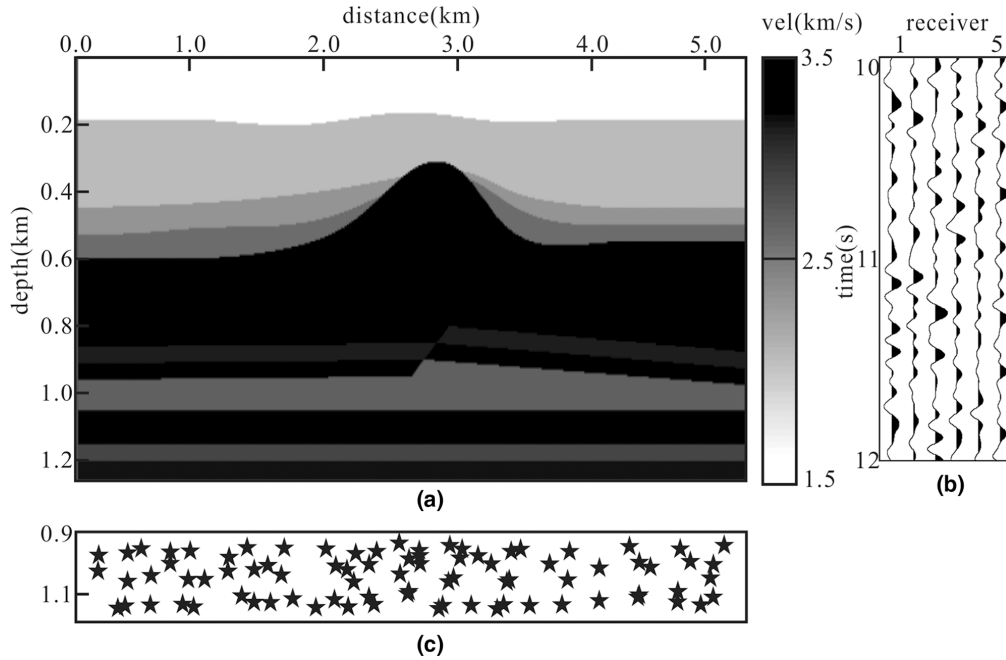


Figure 10 (a) Complex salt model, (b) wavelets of the random sources and (c) distribution of sources.

can see that the proposed method provides accurate primaries and correct travel time at far offsets. Note that the primary estimation from noise-source seismic data and artificial-source data is almost the same. However, because the focal-denoising operator cannot remove all the incoherent noise, we can still observe some noise leakage in Figure 6(a–c). Associated zero-offset profiles are also shown in Figure 9(a–d). It is clear that the primaries are estimated in an accurate and clean manner. Noise-free primary estimation and incoherent noise attenuation are achieved simultaneously.

Salt model

In this section, we will apply the proposed method on data simulated by a more complex salt model (Fig. 10), to make it closer to the real situation. Two hundred and ninety-nine noise sources are randomly set between 900 and 1200 m underground (Fig. 10c), and 250 seismic receivers are located at the surface. Figure 11(a) shows the virtual shot gathers (cross-correlation results) from noise-source data. We can observe that multiples are still visible, and valid signals are overlapped by the incoherent noise in the virtual shot gathers. Figure 11(c) shows the primary estimation from virtual shot gathers by using the proposed method. Figure 11(b) shows the shot gather from the same salt model (Fig. 10a) by tra-

ditional artificial-source acquisition. Primary estimation from artificial-source data by sparse closed-loop SRME is shown in Figure 11(d).

By comparing Figure 11(a,c), the travel-time errors at far offsets have been corrected (white arrow), and the incoherent noise is effectively suppressed (black arrow) simultaneously. By comparing Figure 8(c,d), as expected, estimated results for noise-source data are close to artificial-source primary estimation. Figure 12 depicts the enlarged portion of Figure 11, which demonstrates the effect of the algorithm in travel-time correction and noise removal. However, some artefacts and noise can still be observed in the estimates, but these effects are small if we consider how much valid events are visible in the virtual shot gathers.

Figure 13(a,c) shows the zero-offset section of the virtual shot gathers and its corresponding primary estimation by the proposed method, respectively. Figure 13(b,d) shows the zero-offset section of the artificial-source shot gathers and its corresponding primary estimation by sparse closed-loop SRME. From Figure 13, some remarks can be deduced: (1) SNR (signal noise ratio) has been significantly improved with the application of the proposed method by comparing with Figure 13(a,c). (2) In terms of artificial-source data multiple elimination, primary estimation with the same quality can also be obtained from noise-source data (Fig. 13c,d). The shown

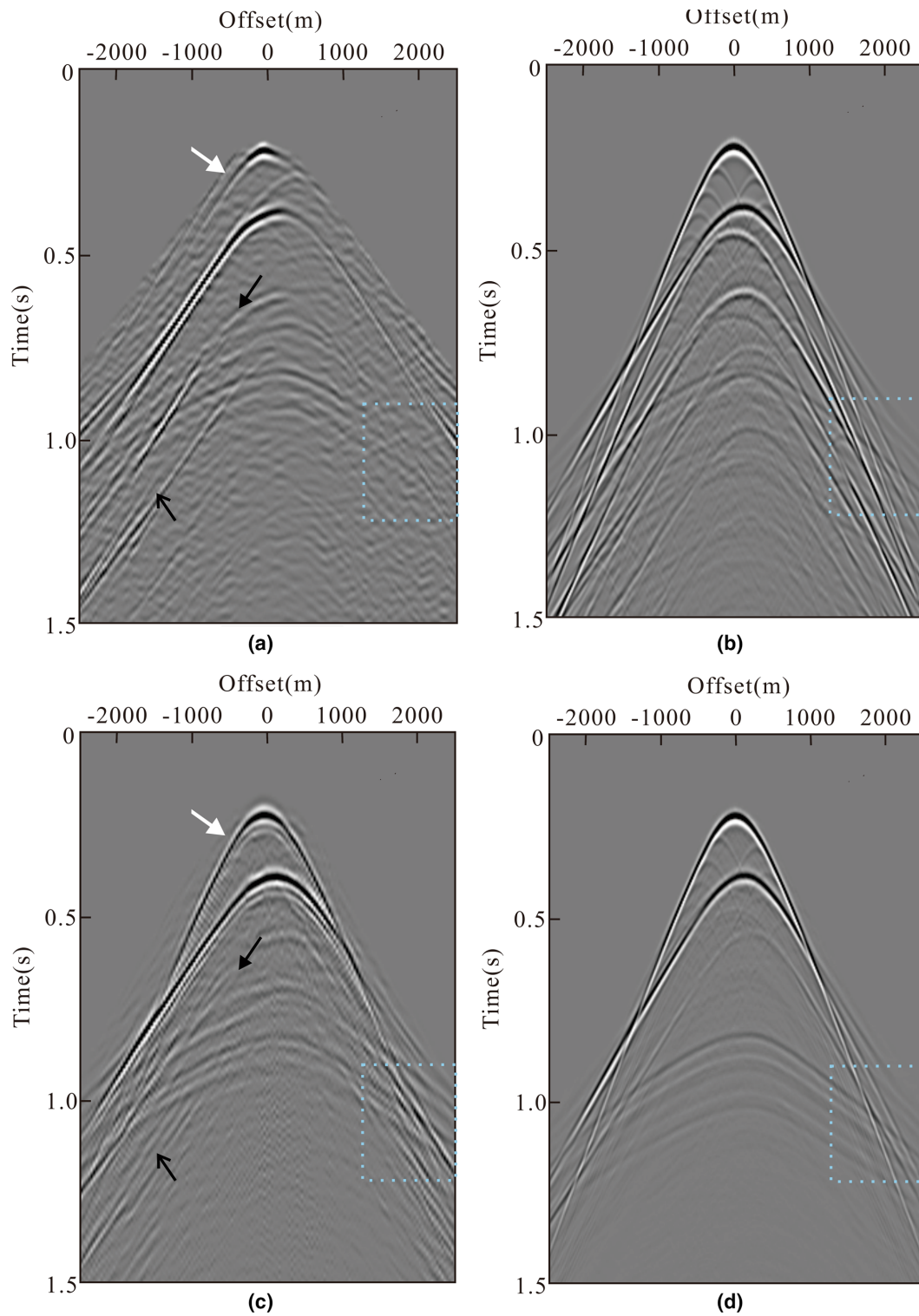


Figure 11 (a) Virtual shot gathers obtained by cross-correlation from noise-source data, (b) active-source data simulated by the same salt model, (c) estimated primary responses from noise-source data by the proposed method, (d) estimated primary responses from active-source data by sparse closed-loop SRME.

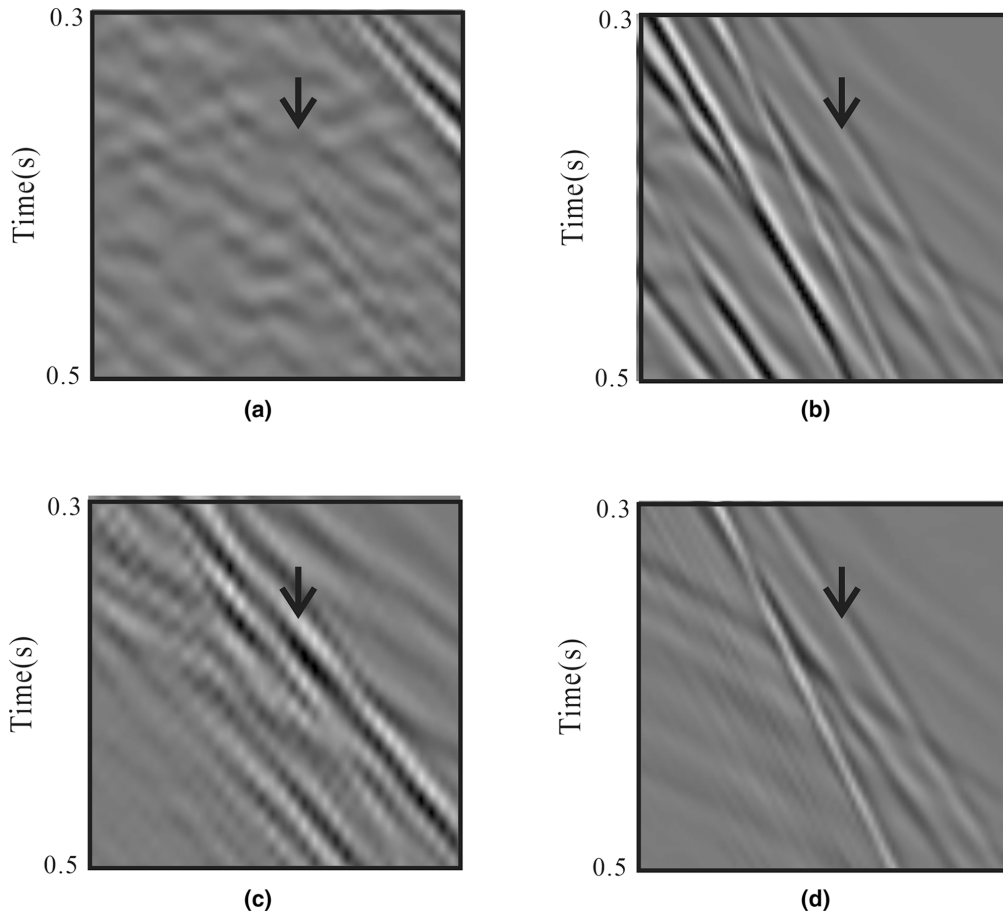


Figure 12 Enlarged portion (red box) of Figure 11.

examples depict capabilities of the present method for noise-source seismic data, in which clean primaries with correct travel time are obtained.

DISCUSSION AND CONCLUSION

The proposed method can be a great value for reservoir monitoring by passive acquisition.

For the synthetic models, we put the sources within a specific range of depth. This setting mimics a situation that reservoir rock cracks during the production. Note, in particular, a prerequisite of our method is that the cross-correlation result must be the input of the algorithm (Draganov *et al.*, 2009).

In terms of the 3D situation, 2D wave propagation can never accurately explain the 3D ray path in practice. Particularly, if there are some dips in the crossline direction, the 2D method cannot estimate accurate primaries, and there will be some multiple leakages in the results. However, all the 3D surface-related multiple elimination (SRME)-related methods,

including our proposed method, are facing an unavoidable problem – computation cost (Dragoset *et al.*, 2010), which need to be further investigated.

In this paper, we have presented the extension of sparse closed-loop SRME to the situation of noise-source data. We combined the focal transform and local similarity into a focal-denoising operator and added it into the conventional sparse closed-loop SRME framework. Our proposed method uses cross-correlation result as the input and estimates noise-free primaries with correct travel time from noise-source data. After this modification, we remove the sensitivity to the limited source illumination and strengths of the noise sources in passive-source acquisition.

ACKNOWLEDGEMENTS

The authors would like to thank the anonymous reviewers for their valuable comments that have helped to improve this paper. This research is supported by the Major Projects

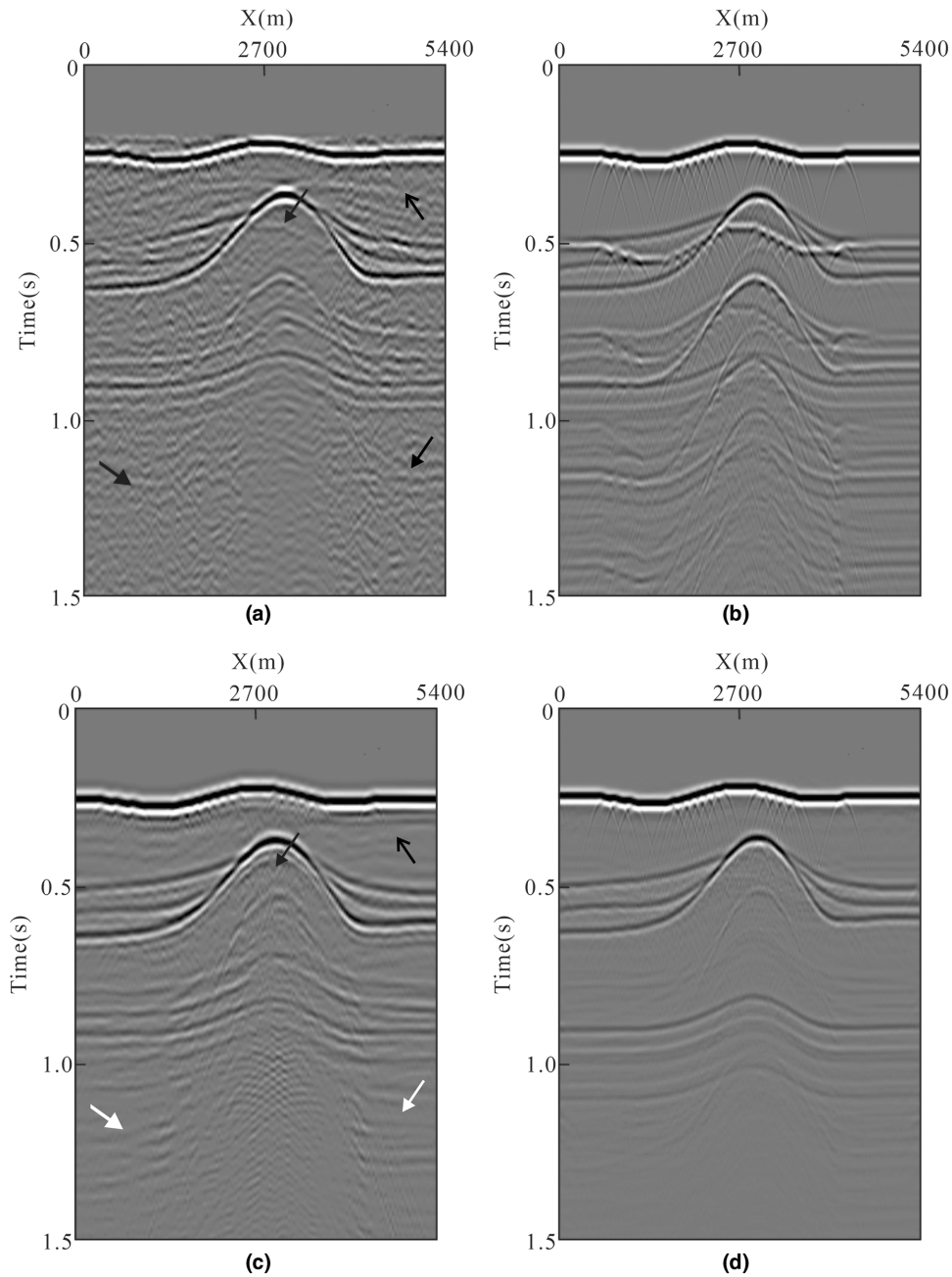


Figure 13 Zero-offset profile of (a) virtual shot gathers from noise-source data, (b) active-source data, (c) estimated primary responses from noise-source data by the proposed method, (d) estimated primary responses from active-source data by sparse closed-loop SRME.

of the National Science and Technology of China (grant no. 2016ZX05026-002-003), the National Natural Science Foundation of China (grant no. 41374108) and China Scholarship Council.

DATA AVAILABILITY STATEMENT

Seismic data used in this paper are the property of Jilin University.

CONFLICTS OF INTEREST

The authors declare that there is no conflict of interest that could be perceived as prejudicing the impartiality of the research reported.

ORCID

Tiexing Wang  <https://orcid.org/0000-0001-8986-4435>

Jing Sun  <https://orcid.org/0000-0002-4660-1106>

REFERENCES

- Berkhout, A.J. (1982) *Seismic Migration: Imaging of Acoustic Energy by Wave Field Extrapolation*. Amsterdam/Oxford/New York: Elsevier Science Publishing Company, pp. 205–211.
- Berkhout, A.J. and Verschuur, D.J. (1997) Estimation of multiple scattering by iterative inversion, part I: Theoretical considerations. *Geophysics*, 62(5), 1586–1595.
- Berkhout, A.J. and Verschuur, D.J. (2006) Focal transformation, an imaging concept for signal restoration and noise removal. *Geophysics*, 71(6), A55–A59.
- Candes, E. and Donoho, D. (2005) Continuous curvelet transform: II. Discretization and frames. *Applied and Computational Harmonic Analysis*, 19(2), 198–222.
- Chen, Y. and Fomel, S. (2014) Random noise attenuation using local similarity. *SEG Technical Program Expanded Abstracts*, Society of Exploration Geophysicists, 4360–4365.
- Cheng, H., Wang, D.L., Feng, F. and Zhu, H. (2015) Estimating primaries from passive seismic data. *Exploration Geophysics*, 46(2), 184–191.
- Clarerbout, J.E. (1968) Synthesis of a layered medium from its acoustic transmission response. *Geophysics*, 33(2), 264–269.
- Daubechies, I. (1992) *Ten Lectures on Wavelets*. Philadelphia, PA: SIAM, pp. 152–155.
- Draganov, D., Campman X., Thorbecke J., Verdel, A. and Wapenaar, K. (2009) Subsurface structure from ambient seismic noise. 71st EAGE Annual International Meeting, Extended Abstracts, Z038.
- Dragoset, B., Verschuur, D.J., Moore, I. and Bisley, R. (2010) A perspective on 3d surface-related multiple elimination. *Geophysics*, 75(5), A245–A261.
- Feng, F., Wang, D.L., Zhu, H. and Cheng, H. (2013) Estimating primaries by sparse inversion of the 3D curvelet transform and the L1-norm constraint. *Applied Geophysics*, 10(2), 201–209.
- Fomel, S. (2007) Local seismic attributes. *Geophysics*, 72(3), A29–A33.
- Hennenfent, G., Berg, E., Friedlander, M.P. and Herrmann, F.J. (2008) New insights into one-norm solvers from the Pareto curve. *Geophysics*, 73(4), A23–A26.
- Hu, B., Wang, D.L., Zhang, L. and Zeng, Z.F. (2019) Rock location and quantitative analysis of regolith at the chang'e 3 landing site based on local similarity constraint. *Remote Sensing*, 11(5), 530–546.
- Lin, T.T.Y. and Herrmann, F.J. (2010) Stabilized estimation of primaries by sparse inversion. 72nd EAGE Conference and Exhibition incorporating SPE EUROPEC, Barcelona, Spain.
- Lin, T.T.Y. and Herrmann, F.J. (2013) Robust estimation of primaries by sparse inversion via one-norm minimization. *Geophysics*, 78(3), R133–R150.
- Lopez, G.A. and Verschuur, D.J. (2014) Closed-loop SRME – a new direction in surface multiple removal algorithms. 76th EAGE Conference and Exhibition, Extended Abstracts, E102.
- Lopez, G.A. and Verschuur, D.J. (2015) Closed-loop surface-related multiple elimination and its application to simultaneous data reconstruction. *Geophysics*, 80(6), V189–V199.
- Ma, J.T., Sen, K.M. and Chen, X.H. (2009) Free-surface multiple attenuation using inverse data processing in the coupled plane-wave domain. *Geophysics*, 74(4), V75–V81.
- Schuster, G.T. (2001) Theory of daylight/interferometric imaging: Tutorial. 63rd EAGE Conference and Exhibition, Amsterdam, the Netherlands, 11th June Extended Abstracts, Session A-32.
- Van den Berg, E. and Friedlander, M.P. (2009) Probing the Pareto frontier for basis pursuit solution. *SIAM Journal on Scientific Computing*, 31(2), 890–912.
- Van den Berg, E. and Friedlander, M.P. (2011) Sparse optimization with least-squares constraints. *SIAM Journal on Optimization*, 21(4), 1201–1229.
- Van Groenestijn, G.J. and Verschuur, D.J. (2009) Estimating primaries by sparse inversion and application to near-offset data reconstruction. *Geophysics*, 74(3), A23–A28.
- Van Groenestijn, G.J. and Verschuur, D.J. (2010) Estimation of primaries by sparse inversion from passive seismic data. *Geophysics*, 75(4), SA61–SA69.
- Vasconcelos, I. and Snieder, R. (2008a) Interferometry by deconvolution: Part 1—Theory for acoustic waves and numerical examples. *Geophysics*, 73(3), S115–S128.
- Vasconcelos, I. and Snieder, R. (2008b) Interferometry by deconvolution: Part 2—Theory for elastic waves and application to drill-bit seismic imaging. *Geophysics*, 73(3), S129–S141.
- Verschuur, D.J., Berkhout, A.J. and Wapenaar, C.P.A. (1992) Adaptive surface-related multiple elimination. *Geophysics*, 57(9), 1166–1177.
- Wang, T.X., Wang, D.L., Sun, J., Hu, B. and Liu, C.M. (2017) Closed-loop SRME based on the 3D L1-norm sparse inversion. *Acta Geophysica*, 65(6), 1145–1152.
- Wapenaar, K. (2004) Retrieving the elastodynamic Green's Function of an arbitrary inhomogeneous medium by cross-correlation. *Physical Review Letters*, 93(25), 254301.
- Wapenaar, K., Van der Neut, J. and Ruigrok, E. (2008) Passive seismic interferometry by multidimensional deconvolution. *Geophysics*, 73(6), A51–A56.
- Wapenaar, K., Draganov, D., Snieder, R., Campman, X. and Verdel, A. (2010a) Tutorial on seismic interferometry. Part I: Basic principles and applications. *Geophysics*, 75(5), A195–A209.
- Wapenaar, K., Slob, E., Snieder, R. and Curtis, A. (2010b) Tutorial on seismic interferometry. Part II: Underlying theory and new advances. *Geophysics*, 75(5), A211–A227.
- Wapenaar, K., Van der Neut, J. and Ruigrok, E. (2011) Seismic interferometry by cross-correlation and by multidimensional deconvolution: A systematic comparison. *Geophysical Journal International*, 185(3), 1335–1364.